ELSEVIER

Comput. Methods Appl. Mech. Engrg. 190 (2000) 757–781

Computer methods in applied mechanics and engineering

www.elsevier.com/locate/cma

A numerical study of a posteriori error estimators for convection–diffusion equations

Volker John

Institut für Analysis und Numerik, Otto-von-Guericke-Universität Magdeburg, Postfach 4120, D-39016 Magdeburg, Germany

Received 29 March 1999

Abstract

This paper presents a numerical study of a posteriori error estimators for convection–diffusion equations. The study involves the gradient indicator, an a posteriori error estimator which is based on gradient recovery, three residual-based error estimators for different norms, and two error estimators which are defined by solutions of local Neumann problems. They are compared with respect to the reliable estimation of the global error and with respect to the accuracy of the computed solutions on adaptively refined grids. The numerical study shows for both criteria of comparison that none of the considered error estimators works satisfactorily in all tests. © 2000 Elsevier Science S.A. All rights reserved.

MSC: 65N50; 65N30

Keywords: Convection-dominated problems; A posteriori error estimation; Adaptive grid refinement

1. Introduction

Scalar convection–diffusion equations describe the transport of a scalar quantity, e.g. temperature or concentration. This transport is composed of a diffusive part and a convective part which dominates in general. The mathematical analysis and the numerical solution of convection-dominated convection–diffusion equations have been of great interest for the last decades, for an overview of the development and the results see [16,18]. The solution of a convection–diffusion equation possesses, in general, layers. These are small subregions where the derivatives of the solution are very large. From their mathematical properties, one distinguishes between regular or exponential boundary layers, parabolic boundary layers, interior layers, and corner layers. The accurate computation of such singularities is of great importance in the numerical solution of convection–diffusion equations.

The use of a posteriori error estimators for estimating the global error as well as for obtaining information for adaptive mesh-refinement techniques is nowadays a standard component in numerical codes for solving partial differential equations. Rigorous analysis of a posteriori error estimators started at the end of the 1970s by the pioneering paper [6]. During the 1980s and at the beginning of the 1990s, fundamental and general approaches for analyzing a posteriori error estimators for finite element solutions of many classes of partial differential equations have been developed, e.g. in [3,4,7,11,19]. However, these techniques often lead to problem-dependent constants in a posteriori error estimates for convection–diffusion equations. These constants may be very large and they may dominate the a posteriori error estimate in such a way that

E-mail address: volker.john@mathematik.uni-magdeburg.de (V. John).

PII: S0045-7825(99)00440-5

Table 1
A posteriori error estimators included in the numerical study

Name	Type	Norm
η_{gradind}	Gradient indicator	
$\eta_{ZZ\text{-}H^1}$	Gradient recovery, Zienkiewicz–Zhu	H^1-semi norm
$\eta_{\text{res-}H^1}$	Residual-based	H^1-semi norm
$\eta_{\text{res-}L^2}$	Residual-based	L^2-norm
$\eta_{\text{res-eng}}$	Residual-based	Energy norm
$\eta_{\text{NeumGa-}H^1}$	Local Neumann problems, Galerkin discretization	H^1-semi norm
$\eta_{\text{NeumSD-}H^1}$	Local Neumann problems, SDFEM discretization	H^1-semi norm

the error estimator does not give reliable information on the error. During the last years, increasing efforts were made in the development of a posteriori error estimators for which the constants in the estimates do not or do only weakly depend on the problem [5,21].

This report presents a numerical comparison of some standard a posteriori error estimators which are often used in the numerical solution of convection–diffusion equations, see Table 1 for an overview of the error estimators. The comparison is twofold. First, the reliability of the error estimators is studied, i.e. the accuracy of the approximation of the true global error. Second, adaptively refined grids are used in order to compute solutions with sharp layers. We compare the quality of the adaptive meshes which are generated by the different error estimators, i.e. the accuracy of the computed solutions on these meshes.

The report is organized as follows: in Section 2, the scalar convection–diffusion equations and their discretization are presented. Section 3 contains a detailed description of the a posteriori error estimators which are studied. In Section 4, we give some general comments to the numerical tests. The numerical tests with respect to the estimation of the global error are presented in Section 5 and with respect to the adaptive grid generation in Section 6. Section 7 summarizes the results of the numerical studies.

2. Scalar convection–diffusion equations

In this section, we give the class of problems we are interested in, describe the finite element discretization of the problems and introduce the notations which will be used in this report.

Let $\Omega \subset \mathbb{R}^2$ be a bounded domain with boundary $\partial\Omega$. We consider scalar convection–diffusion equations

$$\begin{aligned} &-\nabla\cdot\varepsilon\nabla u + b\cdot\nabla u + cu = f \quad \text{in } \Omega,\\ &u = g \quad \text{on } \partial\Omega_D,\\ &\varepsilon\frac{\partial u}{\partial n} = g_N \quad \text{on } \partial\Omega_N, \end{aligned} \tag{1}$$

where the boundary $\partial\Omega = \partial\Omega_D \cup \partial\Omega_N$ is Lipschitz-continuous with $\partial\Omega_D \cap \partial\Omega_N = \emptyset$ and $\text{meas}(\partial\Omega_D) > 0$. The constant ε is positive. The coefficient functions b, c, f and the boundary data g, g_N are assumed to be sufficiently smooth.

For any open subset $\omega \subset \bar{\Omega}$, we denote by $L^2(\omega)$ and $H^k(\omega)$, $k \geqslant 1$, the standard Lebesgue and Sobolev spaces equipped with the norms $\|\cdot\|_{0,\omega} := \|\cdot\|_{L^2(\omega)}$, $\|\cdot\|_{k,\omega} := \|\cdot\|_{H^k(\omega)}$ and the inner product $(\cdot,\cdot)_\omega := (\cdot,\cdot)_{L^2(\omega)}$, see [1]. The energy norm is defined to be $\|\cdot\|_{1,\varepsilon,\omega} := (\varepsilon|\cdot|^2_{1,\omega} + \|\cdot\|^2_{0,\omega})^{1/2}$. If $\omega = \Omega$, we will omit the index ω.

We define $V_0 := \{v \in H^1(\Omega),\ v = 0 \text{ on } \partial\Omega_D\}$. A weak formulation of problem (1) reads as follows:

Find $u \in H^1(\Omega)$ such that $\forall v \in V_0$

$$\begin{aligned} &a(u,v) + b(u,v) + c(u,v) = (f,v) + (g_N,v)_{\partial\Omega_N},\\ &u = g \quad \text{on } \partial\Omega_D, \end{aligned} \tag{2}$$

where

$$a(u,v) = (\varepsilon\nabla u, \nabla v), \quad b(u,v) = (b\cdot\nabla u, v), \quad c(u,v) = (cu, v).$$

Let $\mathscr{T}_h$ be a decomposition of Ω into open triangles. A triangle is denoted by K, its diameter (longest edge) by h_K, an edge by E, and the length of the edge by h_E. We consider only admissible and shape-regular families of triangulations $\{\mathscr{T}_h\}$. A triangulation is called admissible if the intersection of the closure of two triangles is either empty, a common vertex, or a common edge. A family of triangulations is said to be shape-regular if there exists a constant C independent of $\mathscr{T}_h$ such that for all triangulations

$$\frac{h_K}{h_E} \leqslant C \quad \forall K \in \mathscr{T}_h \quad \forall E \subset \partial K.$$

We use the streamline-diffusion finite element method (SDFEM) to discretize (2), [12]. The SDFEM stabilizes a convection-dominated problem by adding weighted residuals to the standard Galerkin finite element method. This corresponds to an addition of artificial viscosity along streamlines. Let $P_1(K)$ be the space of polynomials of degree not greater than 1 defined on the mesh cell K and define the finite element spaces

$$V_h := \{v_h \in H^1(\Omega) : v_h|_K \in P_1(K)\}, \quad V_{h0} := \{v_h \in V_h : v_h|_{\partial\Omega_D} = 0\}.$$

The discrete problem obtained with the SDFEM is the following:
Find $u_h \in V_h$ such that $\forall v_h \in V_{h0}$

$$\begin{aligned} &a(u_h, v_h) + b(u_h, v_h) + c(u_h, v_h) + \sum_{K\in\mathscr{T}_h} \delta_K(-\varepsilon\Delta u_h + b\cdot\nabla u_h + cu_h, b\cdot\nabla v_h)_K \\ &\quad = (f, v_h) + (g_N, v_h)_{\partial\Omega_N} + \sum_{K\in\mathscr{T}_h} \delta_K(f, b\cdot\nabla v_h)_K, \end{aligned} \tag{3}$$

$$u = g \quad \text{on } \partial\Omega_D.$$

A constant δ_K must be chosen for every mesh cell K. Let the cell Peclét number be defined by

$$Pe_K := \frac{\|b\|_{\infty,K} h_K}{2\varepsilon},$$

where $\|\cdot\|_{\infty,K}$ denotes the norm in $(L^\infty(K))^2$. From the analysis of the SDFEM, the following choices of δ_K are optimal:

$$\delta_K = \begin{cases} \delta_0 h_K/\|b\|_{\infty,K} & \text{if } Pe_K > 1 \text{ (convection-dominated)}, \\ \delta_1 h_K^2/\varepsilon & \text{if } Pe_K \leqslant 1 \text{ (diffusion-dominated)}, \end{cases} \tag{4}$$

with appropriate user-chosen constants δ_0 and δ_1, e.g. see [18].

The jump $[|v_h|]_E$ of a function $v_h \in V_h$ across a face E is defined by

$$[|v_h|]_E := \begin{cases} \lim\limits_{t\to+0}\{v_h(x+tn_E) - v_h(x-tn_E)\}, & E \not\subset \partial\Omega, \\ \lim\limits_{t\to+0}\{-v_h(x-tn_E)\}, & E \subset \partial\Omega, \end{cases}$$

where n_E is a normal unit vector on E and $x \in E$. If $E \subset \partial\Omega$, we choose the outer normal, otherwise n_E has an arbitrary but fixed orientation. With that, every edge E which separates two neighbouring triangles K_1 and K_2 is associated with a uniquely oriented normal n_E (for definiteness from K_1 to K_2) and we have $[|v_h|]_E = v_h|_{K_2} - v_h|_{K_1}$.

3. A posteriori error estimators and indicators

This section starts with some general remarks on the tasks and properties of a posteriori error estimators. Its main part is the presentation of the a posteriori error estimators and indicators which are

included in the numerical studies. Last, we mention some a posteriori error estimators which are not studied in this report.

3.1. Tasks and properties of a posteriori error estimators

As a first step in a posteriori error estimation, a norm has to be chosen in which the error should be estimated. The question of what are appropriate norms for error estimation for convection–diffusion equations is still under discussion within the scientific community. In this report, we investigate error estimators for the L^2-norm, the H^1-semi norm, and the energy norm. From $u - u_h \equiv 0$ on $\partial\Omega_D$ and Poincare's inequality follow that the H^1-semi norm of the error is equivalent to its H^1-norm.

A posteriori error estimators estimate the error of the computed discrete solution u_h of (3) and the unknown solution u of the continuous problem (1) in a prescribed norm $\|\cdot\|$ using only information which are available during the solution process, like the discrete solution itself and the data of the problem.

Let η_K be the estimated error on the mesh cell K and $\eta = (\sum_{K\in\mathscr{T}_h} \eta_K^2)^{1/2}$ the estimated global error. The error estimation should be twofold. A global upper estimate

$$\|u - u_h\| \leqslant c\eta \tag{5}$$

gives information on the global error. The global error estimate (5) serves as a stopping criterion of the solution process. Given a required accuracy *tol*, then the discrete solution u_h is sufficiently accurate if $c\eta \leqslant \text{tol}$. Here, the constant c in (5) must be known at least approximately. A local lower estimate

$$\eta_K \leqslant c_K \|u - u_h\|_{U(K)}, \tag{6}$$

where $U(K)$ is a neighbourhood of the mesh cell K, insures a local error where η_K is positive. This justifies, in combination with the assumption that the constants c_K are of the same magnitude for all mesh cells K, the use of a posteriori error estimators for the control of the adaptive grid refinement. Summation of (6) over all mesh cells gives a lower estimate of the global error. In general, (5) and (6) can be proven only with some extra terms on the right-hand side which, for e.g. measure errors coming from the numerical integration of the coefficients of the problem. Using appropriate quadrature rules, these additional terms are of higher order.

Definition 3.1. The efficiency index of an a posteriori error estimator is the ratio of the estimated and the true error

$$I_{\text{eff}} := \frac{\eta}{\|u - u_h\|}.$$

An a posteriori error estimator is called efficient, if I_{eff} and I_{eff}^{-1} are bounded for all triangulations. An efficient a posteriori error estimator is called robust for a class of problems, if I_{eff} and I_{eff}^{-1} are bounded independently of the particular problem, especially independently of the coefficients of the problem.

3.2. The gradient indicator η_{gradind}

The gradient indicator is widely used in software packages for the control of the adaptive grid refinement for the reason of its simplicity. It is defined on the mesh cell K by

$$\eta_{\text{gradind,K}} := \|\nabla u_h\|_{L^2,K},$$

i.e., the indicator is large in mesh cells where the L^2- norm of the gradient of u_h is large. These mesh cells will be refined. The gradient indicator is easy to implement and independent of the class of problems. However, an estimate of the global error is not possible with η_{gradind}.

3.3. The Zienkiewicz–Zhu estimator $\eta_{ZZ\text{-}H^1}$

The Zienkiewicz–Zhu estimator was proposed in [22]. Its aim is to estimate $\|\nabla u - \nabla u_h\|_{L^2(K)}$. For this purpose, a higher-order recovery Gu of ∇u will be constructed using only u_h. If the approximation Gu is more accurate than ∇u_h, i.e.

$$\|\nabla u - Gu\|_{L^2(K)} \leqslant c\|\nabla u - \nabla u_h\|_{L^2(K)}, \quad c < 1,$$

then the two-sided estimate of the true error

$$\frac{1}{1+c}\|Gu - \nabla u_h\|_{L^2(K)} \leqslant \|\nabla u - \nabla u_h\|_{L^2(K)} \leqslant \frac{1}{1-c}\|Gu - \nabla u_h\|_{L^2(K)}$$

is valid. In this case

$$\eta_{ZZ\text{-}H^1,K} := \|Gu - \nabla u_h\|_{L^2(K)} \quad \forall K$$

is an error estimator for the H^1-semi norm.

There are different ways to construct Gu. In general, the function Gu at a point is an average of the gradient of u_h in a neighbourhood of that point. We assume that Gu is completely determined by its values in the nodes of the grid, i.e. in the vertices of the triangles. Thus, we can identify Gu with a continuous and piecewise linear function in each component. Let A be a node of the mesh and ω_A be the union of all mesh cells with node A . Then, $Gu(A)$ is defined as the weighted average of the gradients of u_h of all mesh cells in ω_A

$$Gu(A) = \sum_{K \in \omega_A} \frac{|K|}{|\omega_A|} \nabla u_h|_K,$$

where $|K|$ is the area of K and $|\omega_A|$ the area of ω_A. This error estimator is independent of the class of problems. To our knowledge, there is no analysis for this type of error estimator for convection–diffusion problems.

3.4. A residual-based error estimator in the H^1-semi norm $\eta_{\text{res-}H^1}$

The general form of residual-based a posteriori error estimators for convection–diffusion problems is

$$\eta_{*,K}^2 := \alpha_K \|f_h + \varepsilon\Delta u_h - b_h \cdot \nabla u_h - c_h u_h\|_{0,K}^2 + \sum_{E \subset \partial K,\ E \not\subset \partial\Omega_N} \frac{\beta_E}{2} \|[\![\varepsilon \nabla u_h \cdot n_E]\!]_E\|_{0,E}^2 + \sum_{E \subset \partial K,\ E \subset \partial\Omega_N} \beta_E \|\varepsilon \nabla u_h \cdot n_E - g_{Nh}\|_{0,E}^2, \tag{7}$$

where f_h, b_h, c_h and g_{Nh} are approximations of f, b, c, g_N such that the restriction to each element K of $f_h + \varepsilon\Delta u_h - b_h \cdot \nabla u_h - c_h u_h$ and the restriction of g_{Nh} to each edge $E \subset \partial\Omega_N$ are polynomials of some fixed degree k. The first term of $\eta_{*,K}$ is the norm of the residual of the strong formulation (1) of the convection–diffusion equation. The second term measures the jumps of ∇u_h across edges. The third term measures the error in the Neumann boundary condition.

An a posteriori error estimator for the H^1-semi norm $\eta_{\text{res-}H^1}$ is obtained by choosing $\alpha_K = h_K^2$ and $\beta_E = h_E$. For $\eta_{\text{res-}H^1}$, a global upper estimate (5) and a local lower estimate (6) can be proven for the SDFEM discretization (3), e.g. see [19]. However, the constants in these estimates depend on the data of the problem and for large mesh Peclét numbers they even may depend on the size of the triangles. It turns out that $\eta_{\text{res-}H^1}$ is not robust, see also Section 5.

3.5. A residual-based error estimator in the L^2-norm $\eta_{\text{res-}L^2}$

A residual-based a posteriori error estimator $\eta_{\text{res-}L^2}$ for $\|u - u_h\|_0$ can be obtained by choosing $\alpha_K = h_K^4$ and $\beta_E = h_E^3$ in (7). A local lower estimate of type (6) can be proven with the help of smooth cut-off

functions, see [15,20]. For the standard Galerkin discretization, a global upper estimate (5) can be proven using a duality technique proposed in [11]. The constants in these estimates depend on the mesh size for large mesh Peclét numbers and on the coefficients of the particular problem for small mesh Peclét numbers. Thus, $\eta_{\text{res-}L^2}$ is not robust, which is also demonstrated in Section 5.

3.6. A residual-based error estimator in the energy norm $\eta_{\text{res-eng}}$

In [21], a residual-based a posteriori error estimator for the energy norm $\eta_{\text{res-eng}}$ is defined by choosing $\alpha_K = \min\{h_K^2\varepsilon^{-1}, 1\}$ and $\beta_E = \min\{h_E\varepsilon^{-1}, \varepsilon^{-1/2}\}$ in (7). A global upper estimate (5) and a local lower estimate (6) are proven for the SDFEM discretization (3). In the case of small mesh Peclét numbers, $\eta_{\text{res-eng}}$ is robust. However, for the more interesting case of large mesh Peclét numbers, the constants in the estimates may depend on the coefficients of the problem. The character of this dependence varies with properties of the solution of the particular problem, cf. Section 5.

3.7. An error estimator based on the solution of local Neumann problems, Galerkin discretization, $\eta_{\text{NeumGa-}H^1}$

Error estimation with the solution of local Neumann problems, which are defined on a single mesh cell, was proposed first in [7]. This approach is also called *element residual method* [3,4].

The global error can be represented as the solution of a convection–diffusion equation (1) with the residual as right-hand side. In the element residual method, this global error residual problem is solved approximately in a finite element space consisting of piecewise polynomials of a higher order than the polynomials in V_h. Continuity across edges of these finite element functions is not required.

We consider a mesh cell K with edges $E_i,\ i = 1, 2, 3$. Let λ_{E_i} denote the barycentric coordinates of edge E_i. We define the four-dimensional space on K

$$V_K = \text{span}\{B_K, B_{E_i},\ i = 1, 2, 3\},$$

where B_K is the element bubble function and B_{E_i} are the edge bubble functions defined in K by

$$B_K = 27\lambda_{E_1}\lambda_{E_2}\lambda_{E_3}, \quad B_{E_i} = 4\lambda_{E_{(i+1)\text{modulo}3}}\lambda_{E_{(i+2)\text{modulo}3}}.$$

An approximate solution of the global error residual problem is computed in the space $\cup_{K\in\mathcal{T}_h} V_K$. Because of the discontinuity of the functions in this space, the solution of the global equation can be split into solutions of Neumann problems which are defined in a single mesh cell K:

Find $e_K \in V_K$ such that $\forall v_K \in V_K$

$$a(e_K, v_K) + b(e_K, v_K) + c(e_K, v_K) = (f + \varepsilon\Delta u_h - b\cdot\nabla u_h - cu_h, v_K)_K - \frac{1}{2}\sum_{E,\ E\subset\partial K,\ E\not\subset\partial\Omega} ([|\varepsilon\nabla u_h\cdot n_E|]_E, v_K)_E + \sum_{E,\ E\subset\partial K,\ E\subset\partial\Omega_N} (g - \varepsilon\nabla u_h\cdot n_E, v_K)_E. \tag{8}$$

The right-hand side of the global error residual problem contains the term $-([|\varepsilon\nabla u_h\cdot n_E|]_E, v_K)_E$ for each inner edge E. In the definition of (8), this term is distributed in equal parts to both mesh cells having the common edge E. As local error estimator for the H^1-semi norm, we define

$$\eta_{\text{NeumGa-}H^1,K} := |e_K|_{1,K}.$$

This approach contains two difficulties. First, the continuous local Neumann problem corresponding to (8) is, in general, not solvable since compatibility conditions between the right-hand side and the Neumann boundary data may not be fulfilled. The reason is the simple, problem-independent distribution of $-([|\varepsilon\nabla u_h\cdot n_E|]_E, v_K)_E$ for inner edges. This problem led to the development of more sophisticated and complicated distributions called *equilibrated flux approach* [2,4]. Nevertheless, the discrete problem (8) has a unique solution. Second, (8) is the Galerkin discretization of a possible convection-dominated problem. This discretization is not H^1-stable and the solution e_K may have oscillations.

3.8. An error estimator based on the solution of local Neumann problems, SDFEM discretization, $\eta_{\text{NeumSD-}H^1}$

The problem of the non-stable Galerkin discretization in (8) can be solved by using an additional stabilization in the definition of the local Neumann problems. We use a (simplified) SDFEM discretization:

Find $e_K \in V_K$ such that $\forall v_K \in V_K$

$$\begin{aligned} &a(e_K, v_K) + b(e_K, v_K) + c(e_K, v_K) + \delta_K (b \cdot \nabla e_K + c e_K, b \cdot \nabla v_K)_K \\ &\quad = (f + \varepsilon \Delta u_h - b \cdot \nabla u_h - c u_h, v_K + \delta_K b \cdot \nabla v_K)_K - \frac{1}{2} \sum_{E,\ E \subset \partial K,\ E \not\subset \partial\Omega} ([|\varepsilon \nabla u_h \cdot n_E|]_E, v_K)_E \\ &\qquad + \sum_{E,\ E \subset \partial K,\ E \subset \partial\Omega_N} (g - \varepsilon \nabla u_h \cdot n_E, v_K)_E. \end{aligned}$$

The parameter δ_K is chosen in accordance with (4), where the same values of δ_0 and δ_1 were used as in the stabilization of the global problem. The local a posteriori error estimator in the H^1-semi norm is defined by

$$\eta_{\text{NeumSD-}H^1,K} := |e_K|_{1,K}.$$

To our knowledge, there are no estimates of type (5) and (6) for $\eta_{\text{NeumGa-}H^1}$ and $\eta_{\text{NeumSD-}H^1}$ for convection-dominated convection–diffusion equations.

3.9. Some a posteriori error estimators not considered in this report

Residual-based a posteriori error estimators can be defined also for L^p and $W^{1,p}$-norms, $1 < p < \infty$, see [19,20]. The extension of the other types of error estimators to different norms can be done simply by using these norms in the definition of the error estimators.

In [5], a robust a posteriori error estimator is constructed in a norm which is somewhat weaker than the energy norm and which is defined implicitly by an infinite dimensional variational problem. Thus, the norm can be hardly computed in practice. To compute the error estimate, local Dirichlet problems have to be solved.

In [13], an error indicator which is based on information from a wavelet decomposition of the discrete solution is used as adaptive refinement criterion. The solution u of (1) can be decomposed into a large scale space component and components in wavelet spaces. The solution of the reduced convection–diffusion problem can be represented in the large scale space very well. The absolute values of the wavelet coefficients are larger in a neighbourhood of layers than in regions away from layers. To compute the error indicator, the discrete solution u_h is decomposed instead of u and the wavelet coefficients of this decomposition are used as error indicator.

4. General comments to the numerical studies

In this section, some parameters are explained which are important in the practical application of a posteriori error estimators and some general comments to the numerical tests presented below are given.

For the solution of the discrete problem (3), we apply the program flow depicted in Fig. 1. Within this program flow, some parameters have to be chosen whose values may influence the results of the computations considerably.

The computation starts on an initial grid (level 0). First, an error estimator and a level on which the adaptive grid refinement should start (*max_uni_level*) must be chosen. Up to the *max_uni_level*, uniform grid refinement is applied. The most important features of the solution should be recognizable on the *max_uni_level*, e.g. the position of layers. It depends on the particular problem when this will be achieved. In general, an appropriate *max_uni_level* has to be found by numerical tests. After the computation of the error estimator, every mesh cell K possesses a number $\eta_{*,K}$. With the help of these numbers, it must be decided which mesh cells should be refined or coarsened. In all our experiences, the coarsening of cells is unimportant for stationary problems and an appropriate chosen *max_uni_level*. Given a tolerance *ref_tol* and a reference value $\bar{\eta}$, a mesh cell K will be refined if $\eta_{*,K} \geqslant$ *ref_tol* $\bar{\eta}$. There are several ways to choose $\bar{\eta}$, [14,17]. We use $\bar{\eta} = \max_{K \in \mathcal{T}_h} \eta_{*,K}$. To obtain an efficient adaptive algorithm for the solution of stationary problems,

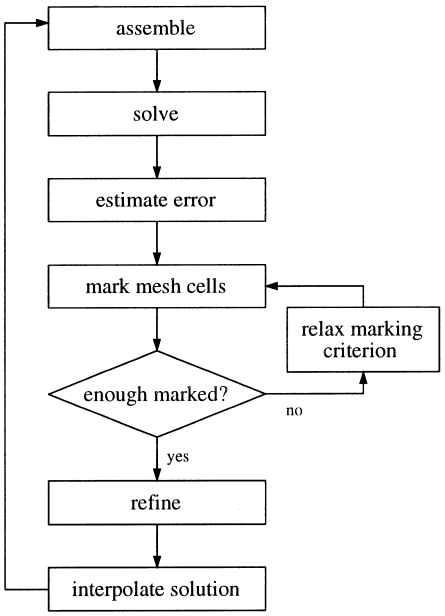

Fig. 1. The program flow.

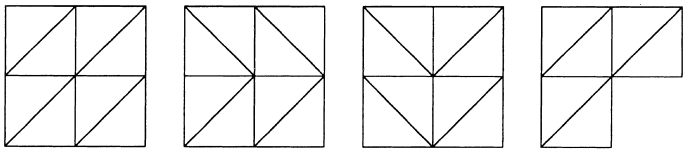

Fig. 2. Coarsest grids for the numerical studies, Grid 1, 2, 3, 4 (left to right).

a sufficient increase of the number of degrees of freedom after an adaptive refinement step is important. This prevents the expensive assembling and solving of a discrete system with only few new degrees of freedom which in general results only in a minor improvement of the discrete solution. We prescribe a minimal amount of mesh cells (in %) which must be marked for refinement (*min_ref*). If not sufficiently many mesh cells are marked for refinement, then we set *ref_tol* := *ref_tol*/1.1 and the mesh cells are marked again.

The following parameters were used in the examples presented in Sections 5 and 6: *max_uni_level* = 3, *ref_tol* = 0.5, *min_ref* = 0.1 (= 10%). It turned out in all tests that this choice of *min_ref* dominated the choice of *ref_tol*, i.e. *ref_tol* had to be decreased several times before enough cells were marked for refinement.

To have a fair comparison of the different a posteriori error estimators, the different adaptive meshes should possess approximately the same number of degrees of freedom. The computations were stopped after the first mesh on which the sum of degrees of freedom (d.f.) and Dirichlet nodes exceeded 100 000. This stopping criterion reflects the fact that the computation terminates if the memory of the computer is exhausted. Loosely speaking, we define the memory to be exhausted after the first computation with more than 100 000 d.f. The errors in the different norms were computed with a 7-point quadrature rule, see [10, (25.19)]. The computations were carried out on simple geometries and the coarsest grids (level 0) presented in Fig. 2. The streamline-diffusion parameters $\delta_0 = 0.5$ and $\delta_1 = 0.25$ in (4) were used in all tests.

5. The estimation of the global error

This section presents numerical tests which study the behaviour of the a posteriori error estimators with respect to the estimation of the global error. First, we consider an example with polynomial solution, second a solution which possesses regular boundary layers, and third a solution with a circular inner layer.

Example 5.1 (*Polynomial solution*). We consider (1) for different values of ε, $b = (3,2)^{\mathrm{T}}$, $c = 2$, $\Omega = (0,1)^2$, $\partial\Omega_D = \partial\Omega$, and $g = 0$. The right-hand side is chosen such that

$$u(x,y) = 100(1-x)^2x^2y(1-2y)(1-y)$$

is the solution. The derivatives of the solution do not depend on ε which is not typical for solutions of convection–diffusion equations. We used uniform refinement starting with the initial Grid 1, Fig. 2, which results in 263 169 d.f. on level 8. The results of the numerical tests are presented in Figs. 3–5.

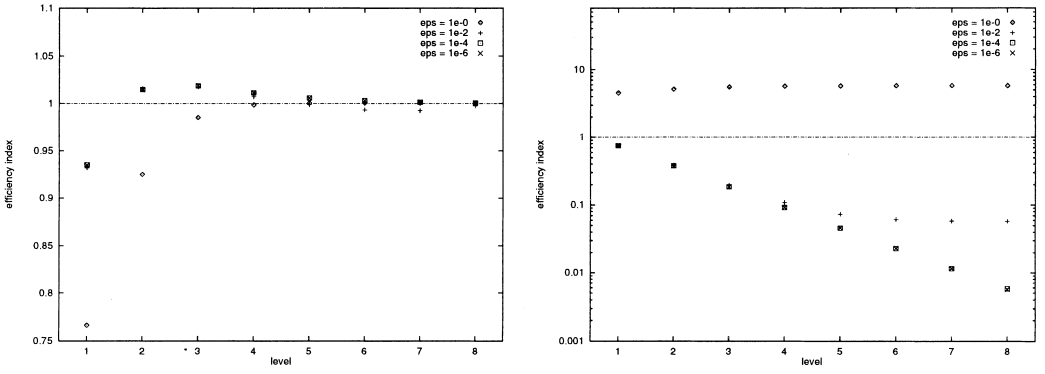

Fig. 3. Efficiency indices, $\eta_{ZZ\text{-}H^1}$ (left) and $\eta_{\text{res-}H^1}$ (right), Example 5.1.

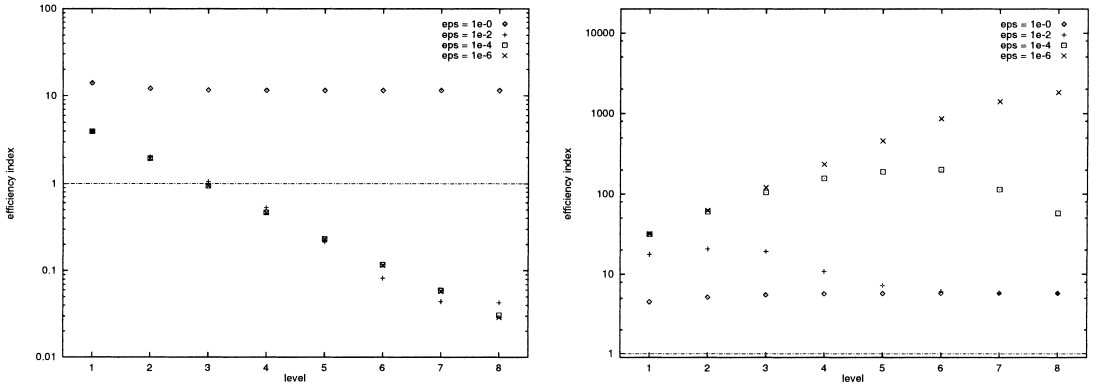

Fig. 4. Efficiency indices, $\eta_{\text{res-}L^2}$ (left) and $\eta_{\text{res-eng}}$ (right), Example 5.1.

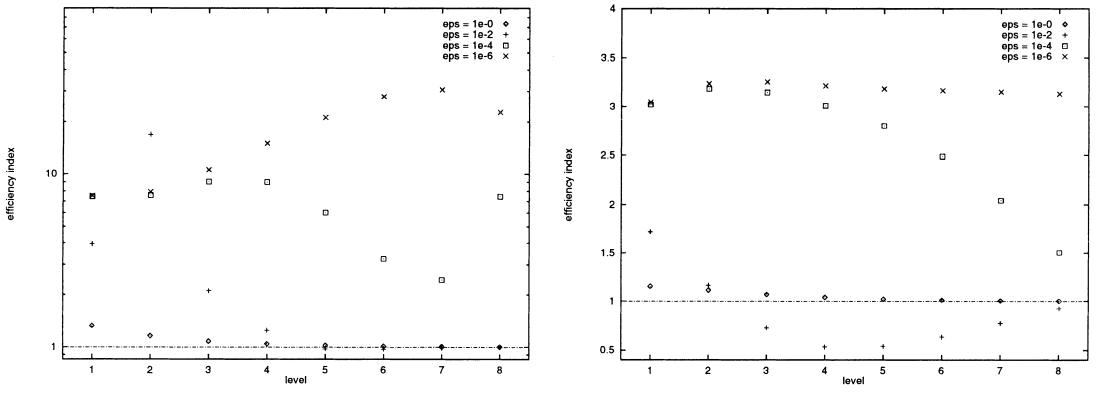

Fig. 5. Efficiency indices, $\eta_{\text{NeumGa-}H^1}$ (left) and $\eta_{\text{NeumSD-}H^1}$ (right), Example 5.1.

The error estimator $\eta_{ZZ\text{-}H^1}$ has efficiency indices close to 1 independent of ε. The global error is estimated very well. Also, the efficiency indices obtained with $\eta_{\text{NeumSD-}H^1}$ are quite good independent of ε. The efficiency indices of $\eta_{\text{NeumGa-}H^1}$ are oscillating somewhat for large mesh Peclét numbers due to the non-stable discretization of the local problems. But the results are still acceptable for all ε. In Example 5.1, all coefficients are constant, the derivatives of the solution do not depend on ε, and all mesh cells have the same size. Thus, the behaviour of the residual-based a posteriori error estimators can be predicted from analytical results. From local lower estimates of type (6) for $\eta_{\text{res-}H^1}$ [19], and $\eta_{\text{res-}L^2}$ [14], follow

$$I_{\text{eff}} \leqslant C \begin{cases} h_K & \text{if } h_K \|b\|_\infty > \varepsilon, \\ \varepsilon & \text{if } h_K \|b\|_\infty \leqslant \varepsilon. \end{cases}$$

The numerical tests confirm these predictions. These error estimators are not robust and the estimated errors do not give reliable information about the true errors. Analogously, the local lower estimate for $\eta_{\text{res-eng}}$, [20], leads to the prediction

$$I_{\text{eff}} \leqslant C \begin{cases} \varepsilon^{-1/2} & \text{if } h_K > \varepsilon^{1/2}, \\ 1 + h_K \varepsilon^{-1} & \text{if } \varepsilon^{1/2} \geqslant h_K > \varepsilon, \\ 1 & \text{if } \varepsilon > h_K. \end{cases}$$

This behaviour can be observed well in the numerical tests. Especially in the most interesting case of large mesh Peclét numbers, $\eta_{\text{res-eng}}$ overestimates the true energy error considerably (see Fig. 4).

Example 5.2 (*Solution with regular boundary layers*). We solve (1) for different values of ε, $b = (2,3)^{\mathrm{T}}$, $c = 1$, $\Omega = (0,1)^2$, and $\partial\Omega_D = \partial\Omega$. The right-hand side and the boundary conditions are chosen such that

$$u(x,y) = xy^2 - y^2 \exp\left(\frac{2(x-1)}{\varepsilon}\right) - x \exp\left(\frac{3(y-1)}{\varepsilon}\right) + \exp\left(\frac{2(x-1)+3(y-1)}{\varepsilon}\right)$$

is the solution, see Fig. 6. The solution possesses typical regular boundary layers at $x = 1$ and $y = 1$.

The computations were carried out on adaptive grids which were generated by the investigated error estimator itself. The accuracy of the solutions on these grids is studied in Example 6.1. We used Grid 1, Fig. 2, as initial grid and present the efficiency indices obtained with the different error estimators in Figs. 7–9.

The efficiency index of $\eta_{ZZ\text{-}H^1}$ behaves for large mesh Peclét numbers like $\mathcal{O}(\varepsilon)$ and converges for small mesh Peclét numbers to 1. However, within the range of about 100 000 d.f., the error is largely underestimated for small ε (see Fig. 7). The error estimator $\eta_{\text{NeumSD-}H^1}$ shows a similar behaviour (see Fig. 9). The situation is much better for $\eta_{\text{NeumGa-}H^1}$. Even for only some 1000 d.f., the error is underestimated less than the factor 5 for all ε. However, we think this is the result of two errors which act in opposite directions and which are of the same order of magnitude in this example. First, the solution of local problems seems to

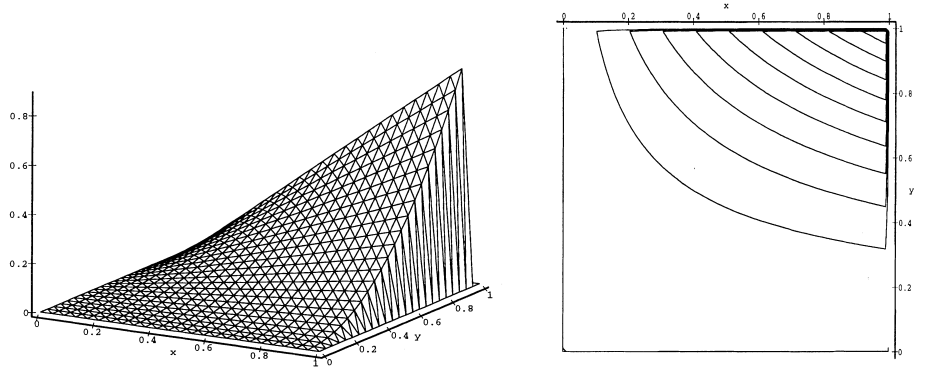

Fig. 6. Solution and contour-lines of Example 5.2, $\varepsilon = 10^{-6}$.

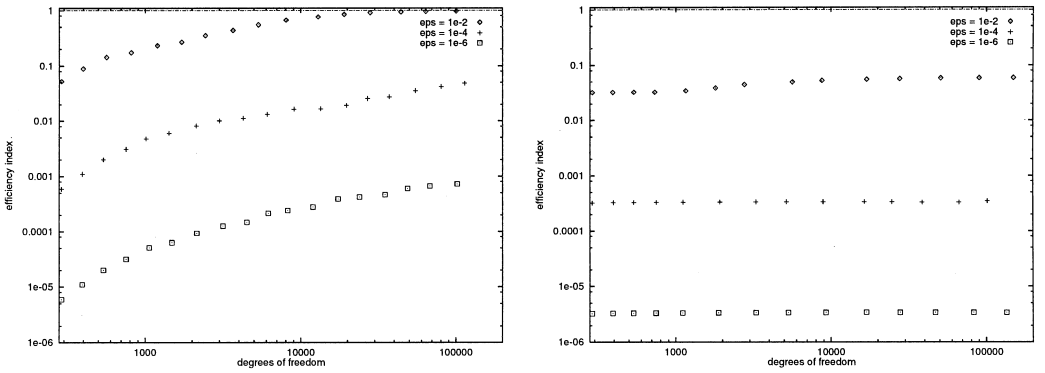

Fig. 7. Efficiency indices, $\eta_{ZZ\text{-}H^1}$ (left) and $\eta_{\text{res-}H^1}$ (right), Example 5.2.

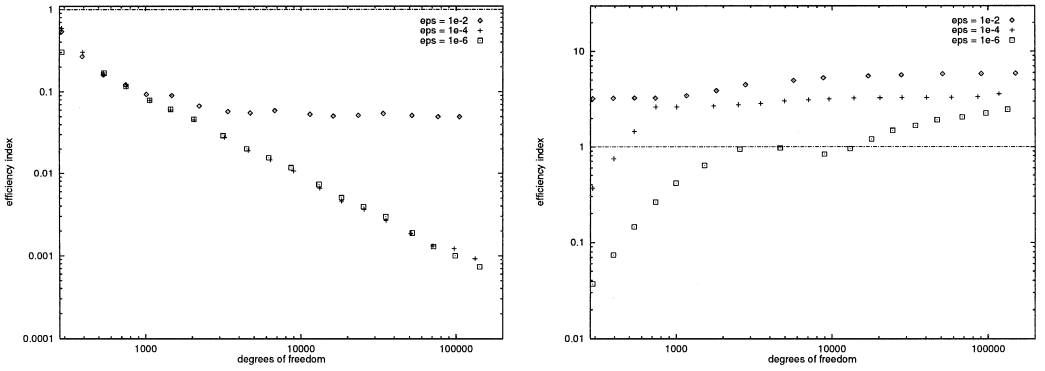

Fig. 8. Efficiency indices, $\eta_{\text{res-}L^2}$ (left) and $\eta_{\text{res-eng}}$ (right), Example 5.2.

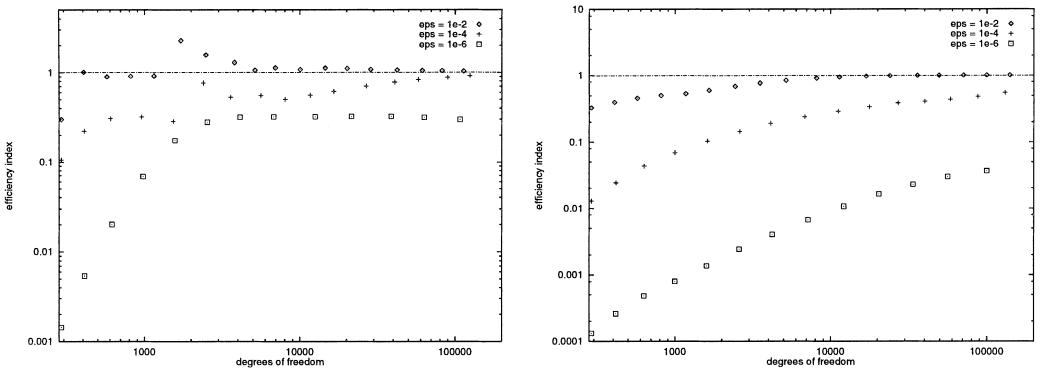

Fig. 9. Efficiency indices, $\eta_{\text{NeumGa-}H^1}$ (left) and $\eta_{\text{NeumSD-}H^1}$ (right), Example 5.2.

lead to a large underestimation of the error for small ε, see $\eta_{\text{NeumSD-}H^1}$. Second, the non-stable discretization of the local problems for computing $\eta_{\text{NeumGa-}H^1}$ leads to oscillating local solutions of (8) and causes a large H^1-semi norm of e_K. This results in an increase of the estimated error. Analytical investigations are necessary to clarify the interaction of these two errors. The error estimators $\eta_{\text{res-}H^1}$ and $\eta_{\text{res-}L^2}$ strongly underestimate the error. In this example, $\eta_{\text{res-}L^2}$ shows the same behaviour as in Example 5.1 whereas the efficiency indices of $\eta_{\text{res-}H^1}$ behave like $\mathcal{O}(\varepsilon)$ for all meshes. In contrast, $\eta_{\text{res-eng}}$ gives reliable error estimates provided the mesh within the boundary layers is sufficiently fine. This is achieved for about 1000 d.f. for all

considered values of ε. The behaviour of the residual-based a posteriori error estimators can be explained with local lower estimates proven in [19–21].

Example 5.3 (*Solution with a circular inner layer*). This example is given by $b = (2,3)^{\mathrm{T}}$, $c = 2$, $\Omega = (0,1)^2$, $\partial\Omega_D = \partial\Omega$, and $g = 0$. The right-hand side is chosen such that

$$u(x,y) = 16x(1-x)y(1-y)\left(\frac{1}{2} + \frac{\arctan[2\sqrt{\varepsilon}(0.25^2 - (x-0.5)^2 - (y-0.5)^2)]}{\pi}\right)$$

is the solution of (1), see Fig. 10. The solution possesses a circular inner layer where its gradient behaves like $\mathcal{O}(\varepsilon^{-1/2})$.

The computations were carried out on adaptively refined grids which were produced by the investigated error estimator itself, starting with Grid 1, Fig. 2, as initial grid. The accuracy of the numerical solutions on these grids is studied in Example 6.2 and the efficiency indices are presented in Figs. 11–13.

The efficiency indices of $\eta_{ZZ\text{-}H^1}$ behave in between Examples 5.1 and 5.2. On one hand, they are close to 1 for all ε. But on the other, the tendency of underestimating the error for large mesh Peclét numbers can be already observed. The residual-based error estimators $\eta_{\text{res-}H^1}$ and $\eta_{\text{res-}L^2}$ underestimate the error in all tests. The underestimation is larger the smaller ε is. The residual-based error estimator $\eta_{\text{res-eng}}$ behaves like in Example 5.1. For large mesh Peclét numbers, it overestimates the error considerably. A similar behaviour shows $\eta_{\text{NeumGa-}H^1}$. The stabilization of the local problems leads to much better results. The efficiency indices with $\eta_{\text{NeumSD-}H^1}$ are good for all values of ε (see Fig. 12).

Remark 5.1. Numerical tests show that the behaviour of the residual-based error estimators can be improved considerably by applying a feed-back approach [8,9]. In this approach, a dual problem with an appropriate right-hand side has to be solved. Important constants arising in the error estimates can be

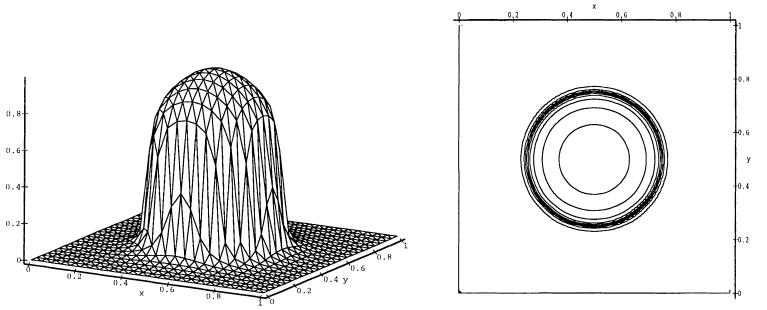

Fig. 10. Solution of Example 5.3, $\varepsilon = 10^{-6}$.

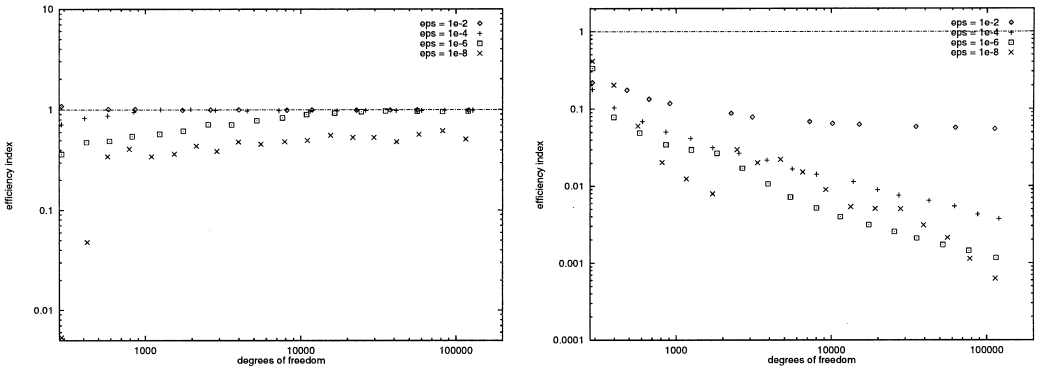

Fig. 11. Efficiency indices, $\eta_{ZZ\text{-}H^1}$ (left) and $\eta_{\text{res-}H^1}$ (right), Example 5.3.

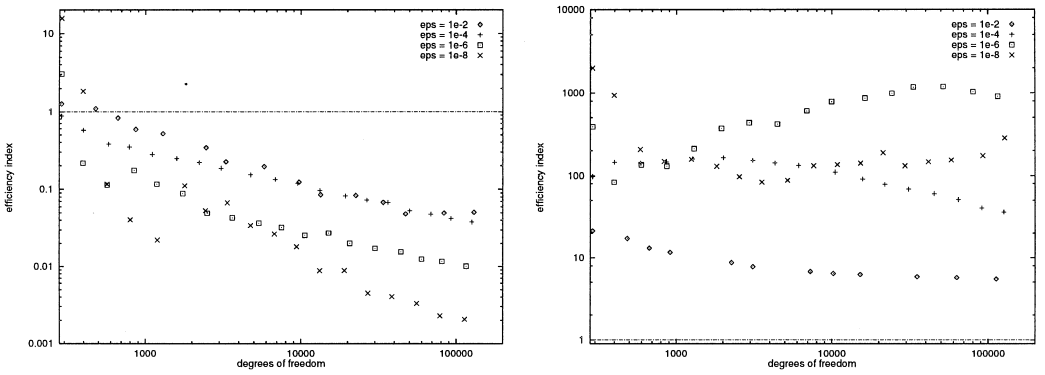

Fig. 12. Efficiency indices, $\eta_{\text{res-}L^2}$ (left) and $\eta_{\text{res-eng}}$ (right), Example 5.3.

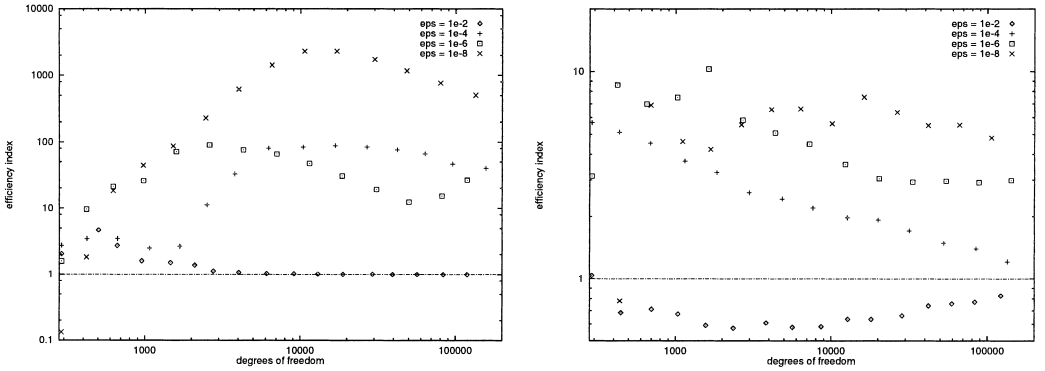

Fig. 13. Efficiency indices, $\eta_{\text{NeumGa-}H^1}$ (left) and $\eta_{\text{NeumSD-}H^1}$ (right), Example 5.3.

estimated with the solution of the dual problem. However, solving the dual problem is approximately as expensive as solving (3).

6. The adaptive grid refinement

This section presents numerical studies of the behaviour of the a posteriori error estimators with respect to the adaptive grid refinement. The examples cover all kinds of singularities which were mentioned in Section 1. In some examples, the solution does not possess the regularity which is assumed in the analysis of some error estimators. However, we think that such examples are of interest since in practical applications, the regularity of the solution is not known in general but appropriate refined grids are also necessary. The error is denoted by $e_h = u - u_h$.

Example 6.1 (*Solution with regular boundary layers*). We consider the same problem with the same parameters in the numerical tests as in Example 5.2.

The errors of the solutions computed on adaptive grids which were generated by the a posteriori error estimators are given in Table 2. The corresponding adaptively refined grids for $\varepsilon = 10^{-6}$ are presented in Figs. 14–16.

The solutions on the grids produced by η_{gradind} are unsatisfactory for all ε. Fig. 14 shows that not the complete boundary layers are refined but only the region where the layers are steepest. A similar behaviour shows $\eta_{\text{ZZ-}H^1}$ for small ε. All residual-based a posteriori error estimators produce adaptively refined grids on which the solutions are much more accurate than for uniform refinement. It can be derived from the

Table 2
Errors of computed solutions on adaptively refined grids, Example 6.1

Estimator	$\varepsilon = 10^{-2}$			$\varepsilon = 10^{-4}$			$\varepsilon = 10^{-6}$		
	d.f.	$\|e_h\|_0$	$\|e_h\|_1$	d.f.	$\|e_h\|_0$	$\|e_h\|_1$	d.f.	$\|e_h\|_0$	$\|e_h\|_1$
Uniform	263 169	3.04 − 3	1.43	263 169	1.60 − 2	318	263 169	1.57 − 2	32 391
η_{gradind}	126 878	1.50 − 3	0.35	161 114	1.40 − 2	277	166 057	2.07 − 2	42 370
$\eta_{\text{ZZ-}H^1}$	100 425	3.42 − 4	0.22	113 621	1.08 − 2	211	101 826	2.76 − 2	53 493
$\eta_{\text{res-}H^1}$	149 842	1.98 − 4	0.18	101 814	1.83 − 3	39	135 545	2.26 − 3	4522
$\eta_{\text{res-}L^2}$	137 957	1.33 − 4	0.21	132 791	2.10 − 3	45	141 850	2.65 − 3	5347
$\eta_{\text{res-eng}}$	149 842	1.98 − 4	0.18	117 265	1.65 − 3	34	133 252	3.40 − 3	6390
$\eta_{\text{NeumGa-}H^1}$	113 514	2.44 − 4	0.21	124 653	1.71 − 3	32	107 608	2.62 − 3	5122
$\eta_{\text{NeumSD-}H^1}$	140 602	2.73 − 4	0.19	130 801	1.69 − 3	34	100 129	7.01 − 3	12953

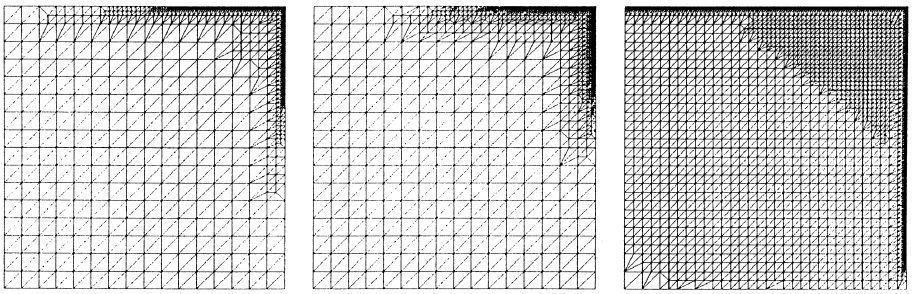

Fig. 14. Mesh with η_{gradind}, $\eta_{\text{ZZ-}H^1}$, $\eta_{\text{res-}H^1}$ (left to right), Example 6.1, $\varepsilon = 10^{-6}$.

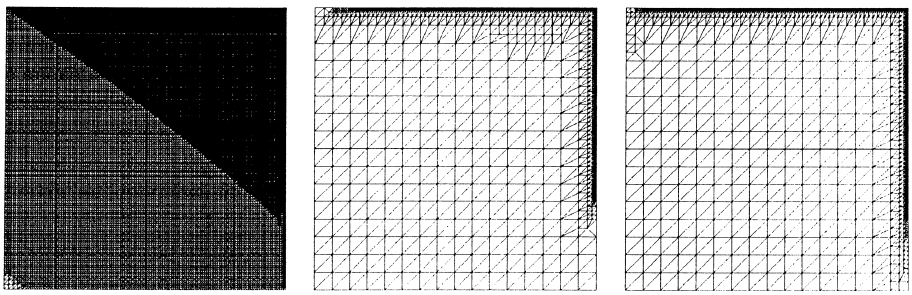

Fig. 15. Mesh with $\eta_{\text{res-}L^2}$, $\eta_{\text{res-eng}}$, $\eta_{\text{NeumGa-}H^1}$ (left to right), Example 6.1, $\varepsilon = 10^{-6}$.

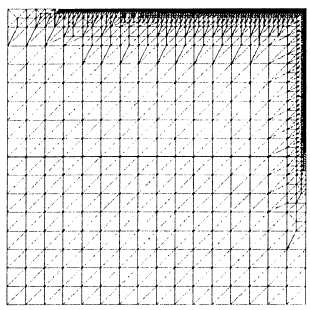

Fig. 16. Mesh with $\eta_{\text{NeumSD-}H^1}$, Example 6.1, $\varepsilon = 10^{-6}$.

weights α_K and β_E of these error estimators that $\eta_{\text{res-}L^2}$ tends to refine large mesh cells earlier than $\eta_{\text{res-}H^1}$, and $\eta_{\text{res-}H^1}$ tends to refine large mesh cells earlier than $\eta_{\text{res-eng}}$. This can be observed very well on the meshes presented in Figs. 14 and 15. The a posteriori error estimator $\eta_{\text{NeumGa-}H^1}$ generates good meshes independently of ε whereas $\eta_{\text{NeumSD-}H^1}$ does not refine within the complete boundary layer for $\varepsilon = 10^{-6}$.

This example shows that some error estimators have problems to produce appropriate adaptively refined grids already in the relatively simple situation that the solution possesses only regular boundary layers.

Example 6.2 (*Solution with a circular inner layer*). This example is described in Example 5.3. The errors of the computed solutions are given in Table 3 and the adaptively refined meshes for $\varepsilon = 10^{-8}$ are presented in Figs. 17–19.

Table 3
Errors of computed solutions on adaptively refined grids, Example 6.2

Estimator	$\varepsilon = 10^{-4}$			$\varepsilon = 10^{-6}$			$\varepsilon = 10^{-8}$		
	d.f.	$\|e_h\|_0$	$\|e_h\|_1$	d.f.	$\|e_h\|_0$	$\|e_h\|_1$	d.f.	$\|e_h\|_0$	$\|e_h\|_1$
Uniform	263 169	6.31 − 5	1.71 − 1	263 169	5.27 − 3	5.81	263 169	1.62 − 1	87.35
η_{gradind}	150 046	3.05 − 4	1.08 − 1	122 656	6.28 − 3	1.29	103 482	4.43 − 1	44.04
$\eta_{ZZ\text{-}H^1}$	128 761	6.48 − 5	7.83 − 2	120 211	3.27 − 4	0.89	115 861	4.66 − 1	49.38
$\eta_{\text{res-}H^1}$	120 021	2.15 − 5	8.76 − 2	114 901	1.10 − 4	0.95	113 612	4.62 − 3	16.99
$\eta_{\text{res-}L^2}$	126 598	2.16 − 5	9.77 − 2	116 059	1.35 − 4	1.17	113 593	5.35 − 3	22.63
$\eta_{\text{res-eng}}$	126 274	2.31 − 5	8.46 − 2	115 342	2.14 − 4	0.93	127 698	2.92 − 1	66.72
$\eta_{\text{NeumGa-}H^1}$	157 203	9.02 − 5	7.66 − 2	118 976	7.56 − 2	22.65	134 782	2.74 − 1	53.66
$\eta_{\text{NeumSD-}H^1}$	134 535	5.19 − 5	9.00 − 2	141 760	3.94 − 4	1.05	106 149	2.01 − 2	29.63

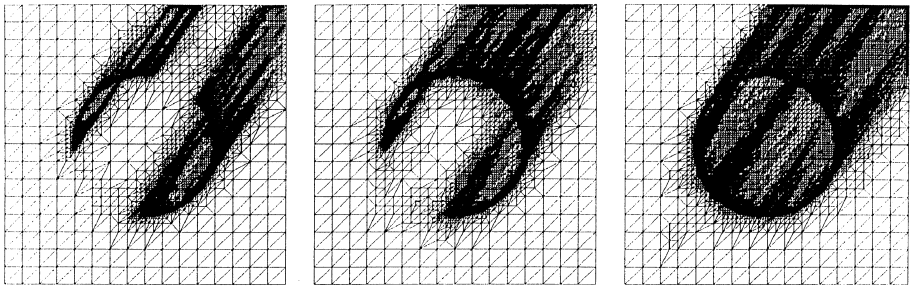

Fig. 17. Mesh with η_{gradind}, $\eta_{ZZ\text{-}H^1}$, $\eta_{\text{res-}H^1}$ (left to right), Example 6.2, $\varepsilon = 10^{-8}$.

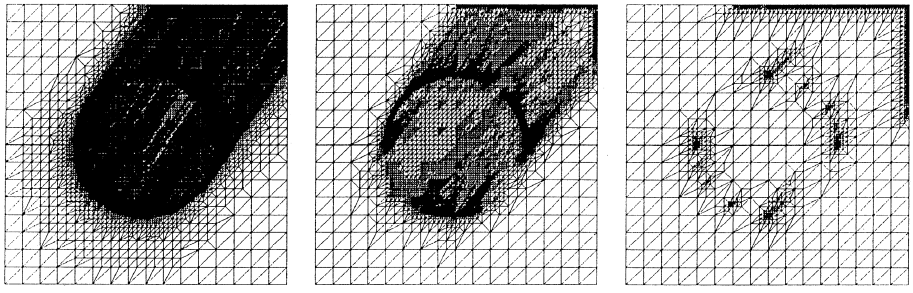

Fig. 18. Mesh with $\eta_{\text{res-}L^2}$, $\eta_{\text{res-eng}}$, $\eta_{\text{NeumGa-}H^1}$ (left to right), Example 6.2, $\varepsilon = 10^{-8}$.

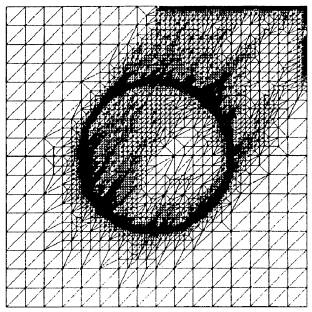

Fig. 19. Mesh with $\eta_{\text{NeumSD-}H^1}$, Example 6.2, $\varepsilon = 10^{-8}$.

The results for $\varepsilon = 10^{-4}$ are satisfying for all error estimators but η_{gradind}. The error estimator $\eta_{\text{NeumGa-}H^1}$ fails completely for $\varepsilon = 10^{-6}$. Instead of refining the region where the inner layer is situated, the outflow boundary is refined like in Fig. 18. For $\varepsilon = 10^{-8}$, $\eta_{\text{res-}H^1}$, $\eta_{\text{res-}L^2}$, and $\eta_{\text{NeumSD-}H^1}$ produce meshes where the region of the inner layer is refined completely. The computed solutions on these meshes are much more accurate than for uniform refinement although they still possess some oscillations. All other error estimators fail to refine appropriately and the computed solutions are of poor quality.

Example 6.3 (*Solution with discontinuous boundary conditions and inner layers*). We consider (1) with $\varepsilon = 10^{-3}$, $b = (1,0)^T$, $c = 0$, $f = 0$, $\Omega = (0,1)^2$ and the boundary condition

$$
\begin{aligned}
&g(x,y) = 0 \quad \text{for} \begin{cases} y = 0 & \text{and} \quad x \leqslant 1, \\ y = 1 & \text{and} \quad x \leqslant 1, \\ x = 0 & \text{and} \quad |y - 0.5| > 0.05, \end{cases} \\
&g(x,y) = 1 \quad \text{for } x = 0 \quad \text{and} \quad |y - 0.5| \leqslant 0.05, \\
&\varepsilon \tfrac{\partial u}{\partial n} \quad = 0 \quad \text{for } x = 1 \text{ and } y \leqslant 1.
\end{aligned}
$$

The solution of this example is

$$
u(x,y) = \sum_{k=1}^{\infty} (\alpha_k \phi_{1k}(x) + \beta_k \phi_{2k}(x)) \psi_k(y) \quad \text{with } \psi_k(y) = \sin(k\pi y)
$$

and

$$
\phi_{1k}(x) = \mathrm{e}^{x/(2\varepsilon)} \frac{\sinh(b_k(1-x))}{\sinh(b_k)}, \quad \phi_{2k}(x) = \mathrm{e}^{(x-1)/(2\varepsilon)} \frac{\sinh(b_k x)}{\sinh(b_k)}, \quad b_k = \sqrt{\frac{1}{(2\varepsilon)^2} + (k\pi)^2}.
$$

The constants are

$$
\alpha_k = \frac{2}{k\pi} (\cos(0.45k\pi) - \cos(0.55k\pi)), \quad \beta_k = \alpha_k \left(\frac{b_k e^{1/(2\varepsilon)}}{\sinh(b_k)} \right) \Big/ \left(\frac{1}{2\varepsilon} + b_k \frac{\cosh(b_k)}{\sinh(b_k)} \right).
$$

For a graphical representation of the solution see Fig. 20. The solution does not belong to $H^1(\Omega)$ due to the jump in the boundary conditions. The computations were carried out on Grid 1, Fig. 2.

The results of the numerical tests are presented in Table 4. Besides the L^2-error and the l^∞-error (node error), we give the error in the midpoint of the outflow boundary. The exact value in this point is $u(1, 0.5) = 0.7368946$.

The H^1-semi norm error estimator $\eta_{\text{res-}H^1}$ generates a mesh which is refined above all near the jumps of the inflow boundary condition. This leads to an insufficient refinement at the interior layers and to the worst discrete solution among all error estimators. Also the solution on the mesh produced by η_{gradind} is not satisfying in comparison to the other results. All other error estimators produce meshes on which the solutions have approximately the same accuracy. The graphical representations of the adaptively refined

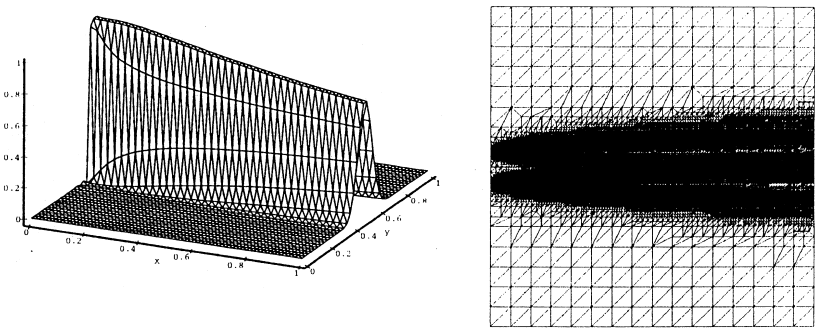

Fig. 20. Solution of Example 6.3 and typical adaptively refined grid ($\eta_{ZZ\text{-}H^1}$).

Table 4
Errors of computed solutions on adaptively refined grids, Example 6.3

Estimator	d.f.	$\|e_h\|_0$	$\|e_h\|_{l^\infty}$	$\|(e_h)(1,0.5)\|$
Uniform	263 169	$5.70-3$	$4.57-3$	$1.28-3$
η_{gradind}	140 051	$5.63-3$	$1.47-3$	$1.36-3$
$\eta_{ZZ\text{-}H^1}$	136 320	$5.54-3$	$6.35-4$	$2.51-4$
$\eta_{\text{res-}H^1}$	124 493	$6.38-3$	$1.71-2$	$1.71-2$
$\eta_{\text{res-}L^2}$	103 818	$5.50-3$	$6.10-4$	$2.08-4$
$\eta_{\text{res-eng}}$	124 360	$5.54-3$	$6.35-4$	$2.72-4$
$\eta_{\text{NeumGa-}H^1}$	103 265	$5.54-3$	$4.41-4$	$2.82-4$
$\eta_{\text{NeumSD-}H^1}$	118 605	$5.54-3$	$6.99-4$	$2.71-4$

grids differ not very much for the different error estimators. A typical grid is presented in Fig. 20. This example demonstrates that several a posteriori error estimators are able to generate appropriate adaptively refined meshes despite the missing regularity of the solution.

Example 6.4 (*Solution with regular boundary layers, corner singularity and inner layer*). We consider an example in the L-shaped domain $(0,1)^2 \setminus [0.5,1] \times [0,0.5]$. The coefficients in (1) are $\varepsilon = 10^{-6},\ b = (3,1)^{\mathrm{T}},\ c = 1,\ f = 100r(r-0.5)(r-\sqrt{2}/2)$ with $r = [(x-0.5)^2 + (y-0.5)^2]^{1/2}$, $\partial\Omega_D = \partial\Omega$, and $g = 0$. An analytical solution of this problem is not known. The solution possesses a corner singularity at $(0.5, 0.5)$, an inner layer in the direction of the convection starting at the corner singularity, and regular boundary layers at $y = 1$, at $\{(0.5,y) : 0 < y \leqslant 0.5\}$, and at $\{(1,y) : 0.5 < y \leqslant 1\}$. Because of the re-entrant corner, $u \notin H^2(\Omega)$.

Grid 4, Fig. 2, was used as coarsest grid. Since we do not know an analytical solution of this problem, we compare the behaviour of the error estimators with graphical representations of the computed solutions and the adaptive grids, see Figs. 21–27. We use as criteria for the quality of the solution the sharpness of the inner layer and the boundary layers.

The error estimators $\eta_{\text{res-}H^1}$ and $\eta_{\text{res-}L^2}$ produce meshes which are well refined within all layers. As a result, the layers in the computed solutions are sharp. The error estimator $\eta_{\text{res-eng}}$ only starts to refine within the inner layer and does not finish the refinement of the boundary layers. Thus, the inner layer is broadly smeared. The position of the inner layer is not found by $\eta_{\text{NeumGa-}H^1}$ and $\eta_{\text{NeumSD-}H^1}$. These error estimators refine only at the corner singularity and within the boundary layers. An insufficient refinement within the inner layer and the boundary layers can be observed on the meshes generated by η_{gradind} and $\eta_{ZZ\text{-}H^1}$. The corresponding discrete solutions are unsatisfactory.

This example shows that most of the studied error estimators have great problems to generate an appropriate mesh if the solution possesses singularities of a different kind. Only two error estimators worked satisfactorily.

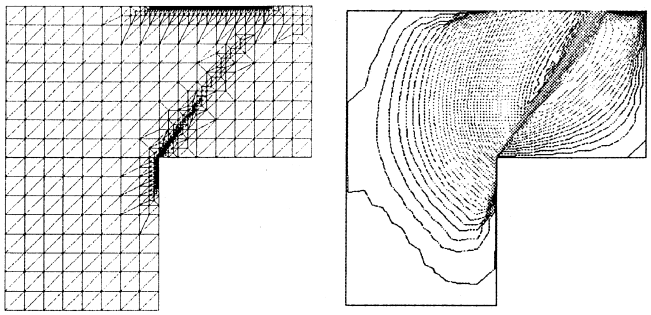

Fig. 21. Mesh and solution obtained with η_{gradind}, Example 6.4.

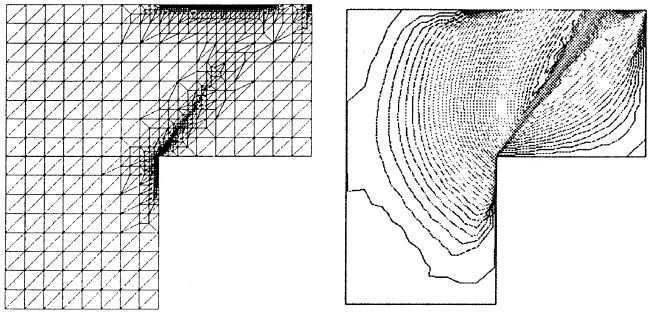

Fig. 22. Mesh and solution obtained with $\eta_{ZZ\text{-}H^1}$, Example 6.4.

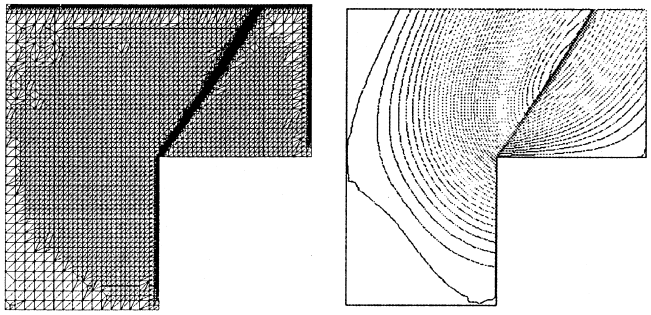

Fig. 23. Mesh and solution obtained with $\eta_{\text{res-}H^1}$, Example 6.4.

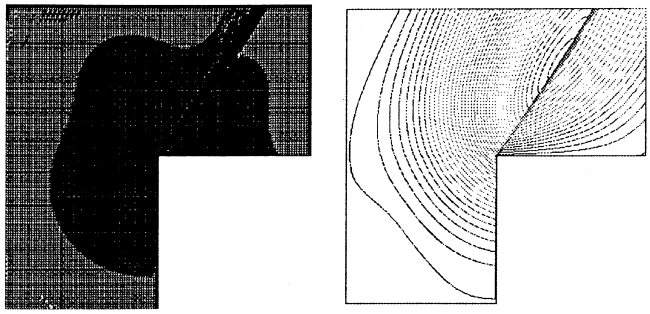

Fig. 24. Mesh and solution obtained with $\eta_{\text{res-}L^2}$, Example 6.4.

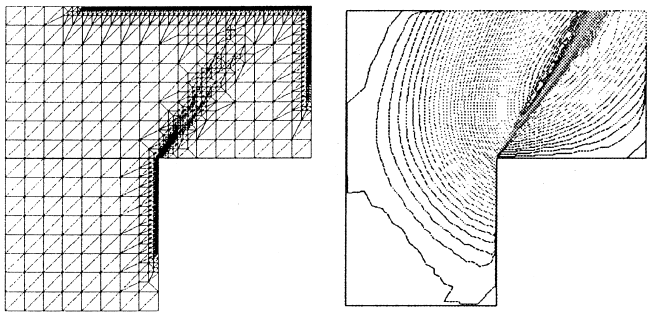

Fig. 25. Mesh and solution obtained with $\eta_{\text{res-eng}}$, Example 6.4.

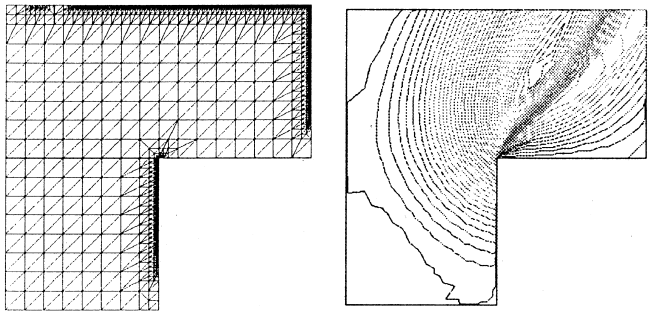

Fig. 26. Mesh and solution obtained with $\eta_{\text{NeumGa-}H^1}$, Example 6.4.

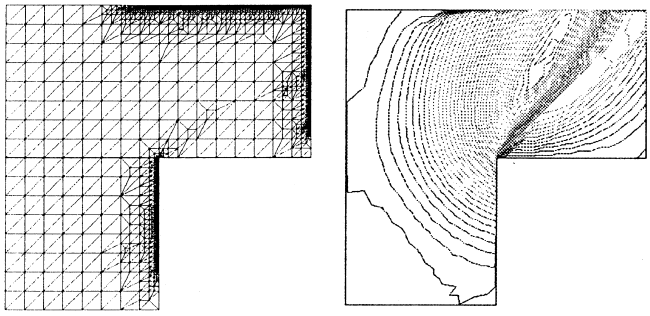

Fig. 27. Mesh and solution obtained with $\eta_{\text{NeumSD-}H^1}$, Example 6.4.

Example 6.5 (*Solution with parabolic and exponential boundary layers*). This example is defined by choosing in (1) $\varepsilon = 10^{-6}$, $b = (1,0)^{\mathrm{T}}$, $c = 0$, $f = 1$, $\Omega = (0,1)^2$, $\partial\Omega = \partial\Omega_D$, and $g = 0$. We do not know an analytical solution of this problem. The solution possesses a regular boundary layer at the outflow boundary $x = 1$ and two parabolic boundary layers at $y = 0$ and $y = 1$.

The computations were carried out on Grid 2, Fig. 2. Since we do not know an analytical solution, we compare the numerical results with graphical representations of the computed solutions, see Figs. 28–34. All error estimators should have no problems to refine within the regular boundary layer which is the strongest singularity in this example. We use as criterion for the quality of the computed solutions the sharpness of the parabolic boundary layers.

Insufficient or no refinement within the parabolic boundary layers can be observed on the meshes produced by η_{gradind}, $\eta_{\text{ZZ-}H^1}$, $\eta_{\text{res-eng}}$, and $\eta_{\text{NeumGa-}H^1}$. The corresponding discrete solutions show broadly smeared parabolic boundary layers. The situation is much better for all other error estimators. The sharpest parabolic layers are obtained on the mesh generated by $\eta_{\text{res-}L^2}$.

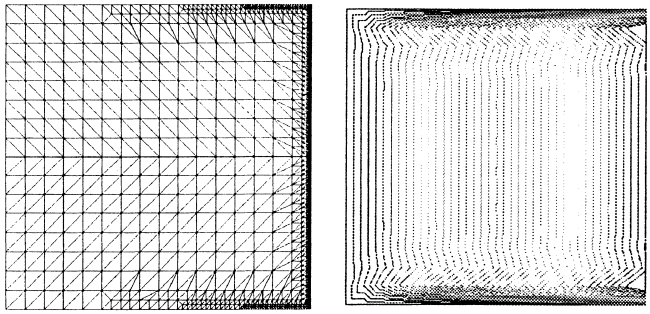

Fig. 28. Mesh and solution obtained with η_{gradind}, Example 6.5.

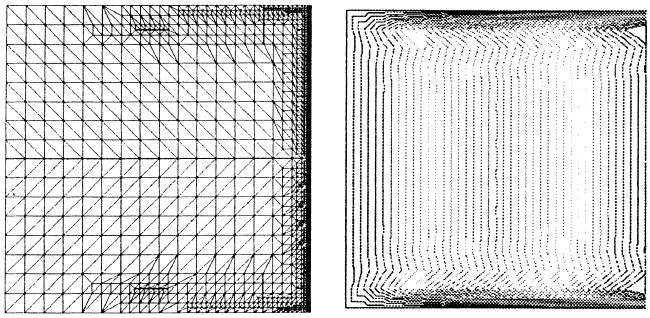

Fig. 29. Mesh and solution obtained with $\eta_{ZZ\text{-}H^1}$, Example 6.5.

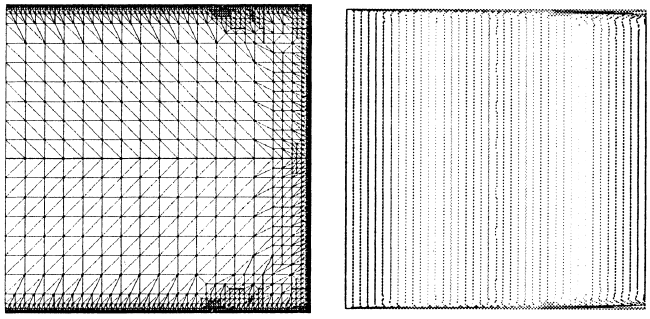

Fig. 30. Mesh and solution obtained with $\eta_{\text{res-}H^1}$, Example 6.5.

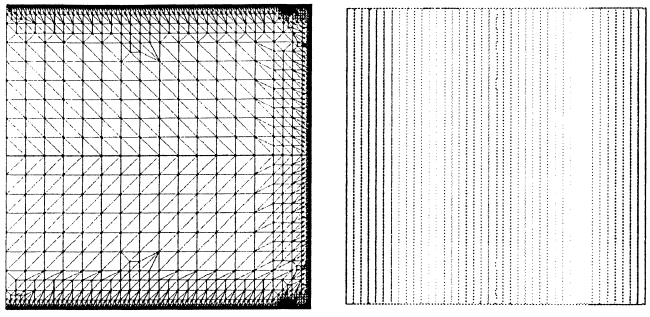

Fig. 31. Mesh and solution obtained with $\eta_{\text{res-}L^2}$, Example 6.5.

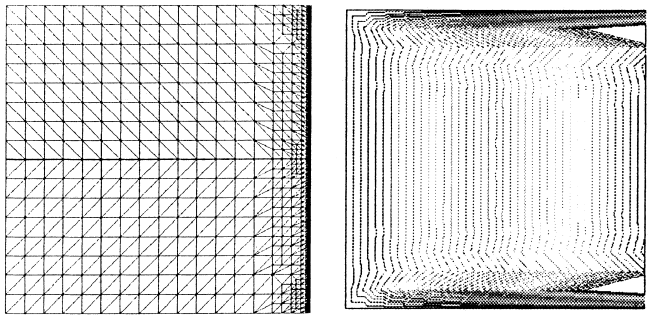

Fig. 32. Mesh and solution obtained with $\eta_{\text{res-eng}}$, Example 6.5.

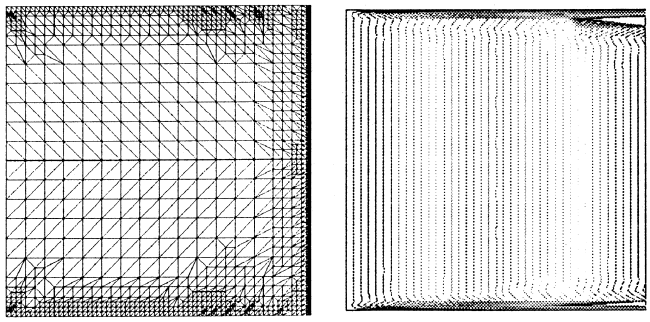

Fig. 33. Mesh and solution obtained with $\eta_{\text{NeumGa-}H^1}$, Example 6.5.

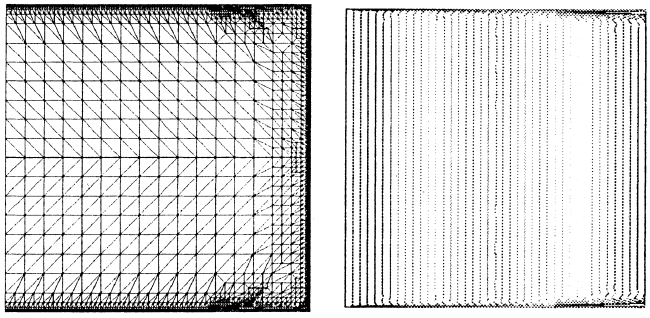

Fig. 34. Mesh and solution obtained with $\eta_{\text{NeumSD-}H^1}$, Example 6.5.

This example demonstrates again the problems of some error estimators to generate appropriate meshes in the presence of singularities of a different kind.

Example 6.6 (*Solution with parabolic and exponential boundary layers, variable convection*). We consider (1) with $\varepsilon = 10^{-6}$, $b = (0, x(1-x))^{\mathrm{T}}$, $c = 0$, $f = x(1-x)y(1-y)$, $\Omega = (0,1)^2$, $\partial\Omega_D = \partial\Omega$, and $g = 0$. An analytical solution of this problem is not known. The solution possesses a regular boundary layer at the outflow boundary $y = 1$ and two parabolic boundary layers at $x = 0$ and $x = 1$.

We used for the computations Grid 3, Fig. 2, as coarsest grid. The numerical results obtained with the different error estimators are compared with graphical representations of the computed solutions, see Figs. 35–42. The sharpness of the parabolic boundary layers as well as the shape of the solution near the regular boundary layer are used as criteria for the quality of the solution.

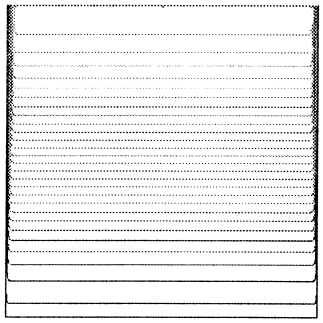

Fig. 35. Computed solution with uniform refinement, Example 6.6.

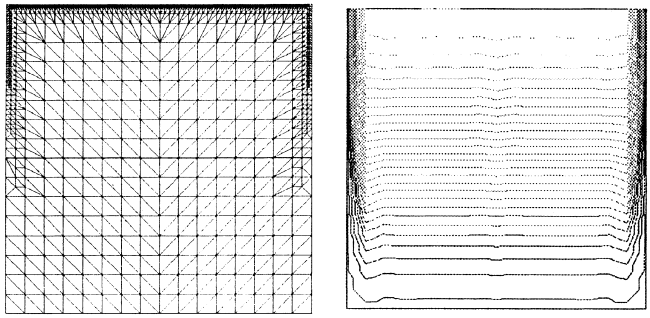

Fig. 36. Mesh and solution obtained with η_{gradind}, Example 6.6.

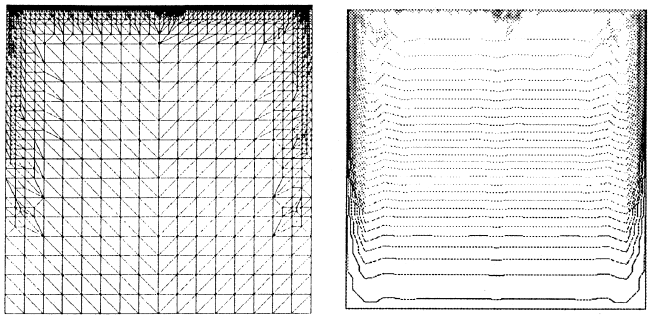

Fig. 37. Mesh and solution obtained with $\eta_{ZZ\text{-}H^1}$, Example 6.6.

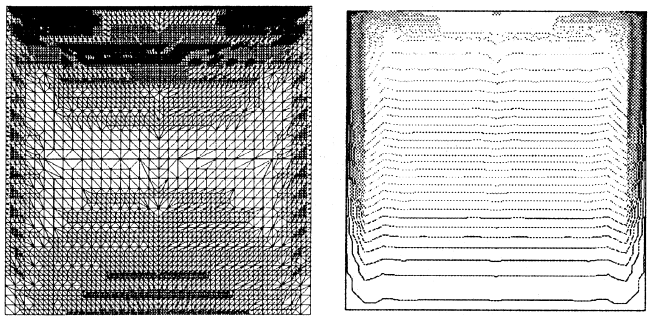

Fig. 38. Mesh and solution obtained with $\eta_{\text{res-}H^1}$, Example 6.6.

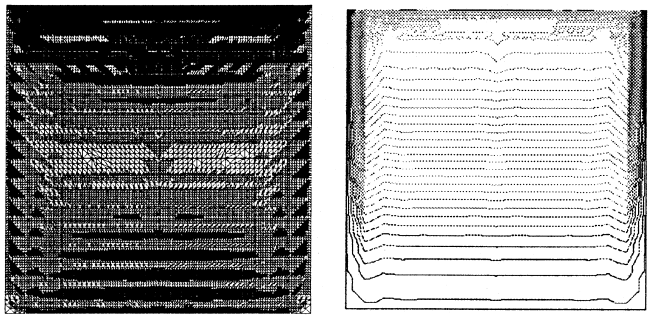

Fig. 39. Mesh and solution obtained with $\eta_{\text{res-}L^2}$, Example 6.6.

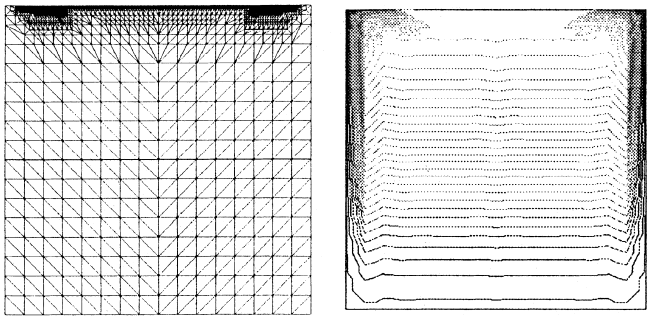

Fig. 40. Mesh and solution obtained with $\eta_{\text{res-eng}}$, Example 6.6.

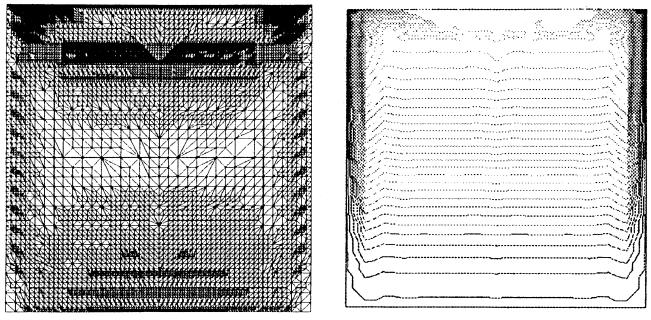

Fig. 41. Mesh and solution obtained with $\eta_{\text{NeumGa-}H^1}$, Example 6.6.

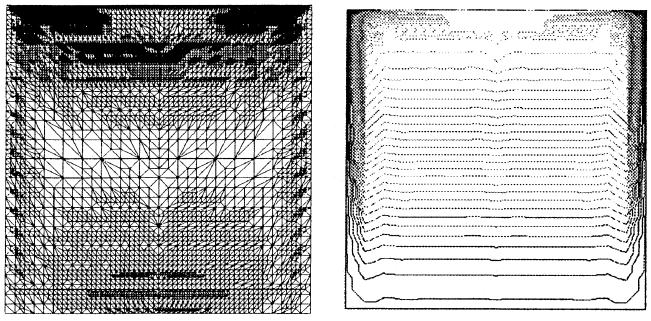

Fig. 42. Mesh and solution obtained with $\eta_{\text{NeumSD-}H^1}$, Example 6.6.

All a posteriori error estimators fail to produce appropriate meshes in this example. Some error estimators do not detect the parabolic layers (η_{gradind}, $\eta_{ZZ\text{-}H^1}$, $\eta_{\text{res-eng}}$). The other error estimators refine in regions where the solution is smooth. All computed solutions on adaptively refined grids are unsatisfactory. The clearly best numerical solution is obtained with uniform refinement, see Fig. 35.

7. Summary

The numerical results are classified into those which we consider as good ones (+), as acceptable ones (○), and as unsatisfactory ones (−).

The behaviour of the error estimators with respect to the estimation of the global error is summarized in Table 5. In examples, in which the derivatives of the solution do not or only slightly depend on ε, $\eta_{ZZ\text{-}H^1}$ and $\eta_{\text{NeumSD-}H^1}$ gave reliable error estimates. If the solution possesses regular boundary layers, the error was estimated reliably by $\eta_{\text{res-eng}}$. But there is no error estimator which worked satisfactorily in all examples. The construction of such an error estimator is still an open problem.

Table 6 summarizes the behaviour of the error estimators with respect to the grid generation. The error estimator $\eta_{\text{res-}L^2}$ worked well in nearly all examples. The meshes produced by $\eta_{\text{res-}L^2}$ are in general more broadly refined then the meshes produced by the other error estimators. This turned out to be better than not finding all subregions of interest for the refinement. The simple gradient indicator η_{gradind} worked unsatisfactorily in all examples. It cannot compete with most of the error estimators. However, even all error estimators failed to work acceptable in Example 6.6. This shows that the problem of the adaptive grid refinement for convection-dominated convection–diffusion equations is not yet completely solved.

Table 5
Behaviour of the error estimators with respect to the estimation of the global error

	Example							
	5.1	5.2			5.3			
ε		10^{-2}	10^{-4}	10^{-6}	10^{-2}	10^{-4}	10^{-6}	10^{-8}
$\eta_{ZZ\text{-}H^1}$	+	+	−	−	+	+	+	+
$\eta_{\text{res-}H^1}$	−	−	−	−	−	−	−	−
$\eta_{\text{res-}L^2}$	−	−	−	−	−	−	−	−
$\eta_{\text{res-eng}}$	−	+	+	+	+	−	−	−
$\eta_{\text{NeumGa-}H^1}$	○	+	+	○	+	−	−	−
$\eta_{\text{NeumSD-}H^1}$	+	+	○	−	+	+	+	+

Table 6
Behaviour of the error estimators with respect to the adaptive mesh generation

	Example									
	6.1			6.2			6.3	6.4	6.5	6.6
ε	10^{-2}	10^{-4}	10^{-6}	10^{-4}	10^{-6}	10^{-8}				
η_{gradind}	○	−	−	○	○	−	○	−	−	−
$\eta_{ZZ\text{-}H^1}$	+	−	−	+	+	−	+	−	−	−
$\eta_{\text{res-}H^1}$	+	+	+	+	+	+	−	+	○	−
$\eta_{\text{res-}L^2}$	+	+	+	+	+	+	+	+	+	−
$\eta_{\text{res-eng}}$	+	+	+	+	+	−	+	−	−	−
$\eta_{\text{NeumGa-}H^1}$	+	+	+	+	−	−	+	−	−	−
$\eta_{\text{NeumSD-}H^1}$	+	+	○	+	+	○	+	−	○	−

The numerical costs of computing the error estimators were different. The cheapest error estimator was η_{gradind}. The computation of $\eta_{ZZ\text{-}H^1}$ was about twice as expensive, the computation of the residual-based error estimators 3–4 times, and the computation of the error estimators based on the solution of local problems 11–12 times. However, the computation of all error estimators was fast in comparison to the solution of the discrete problems.

References

[1] R.A. Adams, Sobolev Spaces, Academic Press, New York, 1975.
[2] M. Ainsworth, J.T. Oden, A posteriori error estimators for second order elliptic systems Part 2. An optimal order process for calculating self equilibrated fluxes, Comput. Math. Appl. 26 (1993) 75–87.
[3] M. Ainsworth, J.T. Oden, A unified approach to a posteriori error estimation using element residual methods, Numer. Math. 65 (1993) 23–50.
[4] M. Ainsworth, J.T. Oden, A posteriori error estimation in finite element analysis, Comput. Meth. Appl. Mech. Engrg. 142 (1997) 1–88.
[5] L. Angermann, Balanced a posteriori error estimates for finite-volume type discretizations of convection-dominated elliptic problems, Computing 55 (1995) 305–323.
[6] I. Babuška, W.C. Rheinboldt, Error estimates for adaptive finite element computation, SIAM J. Numer. Anal. 15 (4) (1978) 283–301.
[7] R.E. Bank, A. Weiser, Some a posteriori error estimators for elliptic partial differential equations, Math. Comp. 44 (1985) 283–301.
[8] R. Becker, R. Rannacher, A feedback approach to error control in finite element methods: basic analysis and examples, East–West J. Numer. Math. 4 (4) (1996) 237–264.
[9] R. Becker, R. Rannacher, Weighted a posteriori error control in FE methods, in: H.G. Bock et al. (Ed.), ENUMATH 97 – Proceedings of the Second European Conference on Numerical Mathematics and Advanced Applications, World Scientific, Singapore, 1998, pp. 621–637.
[10] P.G. Ciarlet, Basic error estimates for elliptic problems, in: P.G. Ciarlet, J.L. Lions (Eds.), Handbook of Numerical Analysis II, North-Holland, Amsterdam, 1991, pp. 19–351.
[11] K. Eriksson, D. Estep, P. Hansbo, C. Johnson, Introduction to adaptive methods for differential equations, Acta Numerica (1995) 105–158.
[12] T.J.R. Hughes, A.N. Brooks, A multidimensional upwind scheme with no crosswind diffusion, in: T.J.R. Hughes (Ed.), Finite Element Methods for Convection Dominated Flows AMD, vol. 34, ASME, New York, 1979.
[13] U. Iben, Eine adaptive Strategie zur Lösung von Konvektion–Diffusion–Gleichungen auf der Basis von Waveletdekompositionen, Ph.D. thesis, TU Dresden, 1998.
[14] V. John, Parallele Lösung der inkompressiblen Navier–Stokes Gleichungen auf adaptiv verfeinerten Gittern. PhD thesis, Otto-von-Guericke-Universität Magdeburg, Fakultät für Mathematik, 1997.
[15] V. John, A posteriori L^2-error estimates for the nonconforming P_1/P_0-finite element discretization of the Stokes equations, J. Comput. Appl. Math. 96 (2) (1998) 99–116.
[16] K.W. Morton, Numerical Solution of Convection–Diffusion Problems, Kluwer Academic Publishers, Dordrecht, 1995.
[17] A. Papastavrou, Adaptive Finite Element Methoden für Konvektions–Diffusions-Probleme, Ruhr-Universität Bochum, 1998.
[18] H.-G. Roos, M. Stynes, L. Tobiska, Numerical Methods for Singularly Perturbed Differential Equations, Springer, Berlin, 1996.
[19] R. Verfürth, A Review of a Posteriori Error Estimation and Adaptive Mesh-Refinement Techniques, Wiley and Teubner, 1996.
[20] R. Verfürth, A posteriori error estimates for nonlinear problems. L^r-estimates for finite element discretizations of elliptic equations, Math. Comp. 67 (224) (1998) 1335–1360.
[21] R. Verfürth, A posteriori error estimators for convection–diffusion equations, Numer. Math. 80 (1998) 641–663.
[22] O.C. Zienkiewicz, J.Z. Zhu, A simple error estimator and adaptive procedure for practical engineering analysis, Internat. J. Numer. Meth. Engrg. 24 (2) (1987) 337–357.